

# Pronounced Microheterogeneity in a Sorbitol–Water Mixture Observed through Variable Temperature Neutron Scattering

Shin G. Chou,<sup>†</sup> Alan K. Soper,<sup>‡</sup> Sheila Khodadadi,<sup>†</sup> Joseph E. Curtis,<sup>†</sup> Susan Krueger,<sup>†</sup> Marcus T. Cicerone,<sup>†</sup> Andrew N. Fitch,<sup>§</sup> and Evgeniy Y. Shalaev<sup>\*,||,##,⊥</sup>

<sup>†</sup>National Institute of Standards and Technology, Gaithersburg, Maryland 20899, United States

<sup>‡</sup>ISIS Facility, Rutherford Appleton Laboratory, Chilton, Didcot, Oxon, OX11 0QX, United Kingdom

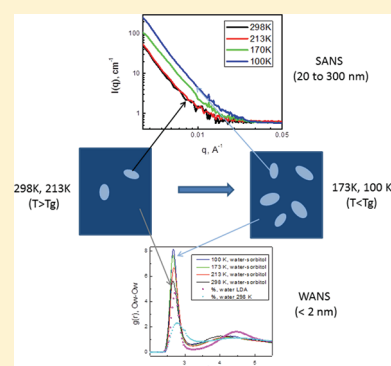
<sup>§</sup>European Synchrotron Radiation Facility, Grenoble, France

<sup>||</sup>Pfizer Incorporated, Groton, Connecticut 06340, United States

<sup>#</sup>Department of Pharmaceutics, University of Minnesota, Minnesota 55455, United States

## Supporting Information

**ABSTRACT:** In this study, the structure of concentrated D-sorbitol–water mixtures is studied by wide- and small-angle neutron scattering (WANS and SANS) as a function of temperature. The mixtures are prepared using both deuterated and regular sorbitol and water at a molar fraction of sorbitol of 0.19 (equivalent to 70% by weight of regular sorbitol in water). Retention of an amorphous structure (i.e., absence of crystallinity) is confirmed for this system over the entire temperature range, 100–298 K. The glass transition temperature,  $T_g$ , is found from differential scanning calorimetry to be approximately 200 K. WANS data are analyzed using empirical potential structure refinement, to obtain the site–site radial distribution functions (RDFs) and coordination numbers. This analysis reveals the presence of nanoscaled water clusters surrounded by (and interacting with) sorbitol molecules. The water clusters appear more structured compared to bulk water and, especially at the lowest temperatures, resemble the structure of low-density amorphous ice (LDA). Upon cooling to 100 K the peaks in the water



RDFs become markedly sharper, with increased coordination number, indicating enhanced local (nanometer-scale) ordering, with changes taking place both above and well below the  $T_g$ . On the mesoscopic (submicrometer) scale, although there are no changes between 298 and 213 K, cooling the sample to 100 K results in a significant increase in the SANS signal, which is indicative of pronounced inhomogeneities. This increase in the scattering is partly reversed during heating, although some hysteresis is observed. Furthermore, a power law analysis of the SANS data indicates the existence of domains with well-defined interfaces on the submicrometer length scale, probably as a result of the appearance and growth of microscopic voids in the glassy matrix. Because of the unusual combination of small and wide scattering data used here, the present results provide new physical insight into the structure of aqueous glasses over a broad temperature and length scale, leading to an improved understanding of the mechanisms of temperature- and water-induced (de)stabilization of various systems, including proteins, pharmaceuticals, and biological objects.

## INTRODUCTION

Systems rich in polyhydroxy compounds (i.e., sugars and sugar alcohols) are widely represented in pharmaceutical and food systems, as well as biological organisms. Sugars have been shown to be effective in protecting both single- and multicellular organisms against environmental stresses such as exposure to subzero temperatures or prolonged drought.<sup>1</sup> In the pharmaceutical and food industry, sugars and sugar alcohols are common cryoprotectors and lyoprotectors, which are used to improve stability of biological and pharmaceutical products during processing (e.g., freezing and drying) and storage.<sup>2</sup> Even though the detailed mechanisms of how these compounds stabilize proteins and other biological systems during freezing and dehydration remain unclear, both their readiness to form solid amorphous (glassy) state and their extensive hydrogen-bonding capacity are believed to contribute to their protective

properties. During the freezing of a typical protein solution, only a fraction of the water molecules form the crystalline hexagonal ice, whereas the remaining water molecules and all of the other solutes present (including sugar and protein molecules) remain in the amorphous state, forming a freeze-concentrated solution, with a water concentration of around 30% by weight (wt %).<sup>3</sup> The frozen system may be further dehydrated under vacuum, first to sublime the ice and then to desorb the unfrozen water from the freeze-concentrated solution, resulting in an amorphous freeze-dried (lyophilized) product with a residual water content of a few weight percent.<sup>4</sup> Even though the freezing event (i.e., ice formation) is often

Received: December 30, 2011

Revised: March 14, 2012

Published: March 26, 2012

associated with protein unfolding, possibly as a result of protein sorption at the ice interface,<sup>5a</sup> trapping protein molecules inside growing ice crystals,<sup>6</sup> or mechanical stresses due to volume expansion,<sup>5b</sup> various physical and chemical processes occurring in the amorphous freeze-concentrate contribute significantly to the destabilization and inactivation of protein molecules. Therefore, a detailed characterization of the structure of amorphous sugars and sugar alcohols and the distribution of water molecules in the glassy matrix at temperatures relevant to cryopreservation is essential to both designing stable biopharmaceutical products and understanding the mechanisms for cryo- and lyoprotection of biological systems.

Although concentrated sugar solutions and glasses lack long-range translational symmetry, they possess a certain degree of short-range correlation. One important aspect of studying the structure of these systems is to characterize the distribution of water molecules in the amorphous glassy matrix. Previous experimental studies have suggested that water molecules can form pockets, or clusters, under certain conditions.<sup>7a</sup> In addition, important insights into the structure of amorphous carbohydrate–water systems have been obtained from molecular dynamics simulation studies. In several simulations of concentrated water–monosaccharide<sup>7b,8</sup> and water–sucrose solutions,<sup>9</sup> spatially isolated water clusters were found at lower water content, whereas the clusters become interconnected when the water concentration was above a percolation threshold. For the glucose–water system at 340 K, for example, the percolation threshold was estimated to be 18 wt %.<sup>8b</sup> In another molecular dynamics simulation study,<sup>10</sup> water clusters (identified as a set of water molecules connected to each other by at least one hydrogen bond with a defined geometric criterion) were studied in three disaccharides with concentrations of up to 66 wt % at relatively high temperatures, above 273 K. The water clusters were found to consist of approximately 20 water molecules at 66 wt % sugar concentration.<sup>10</sup> Separately, these computational studies provided important insight on the structure of concentrated solutions of sugars and sugar alcohols on the subnanometer and nanometer length scale. However, very few experimental investigations of the structure of carbohydrate glasses have been carried out over broad length scales both in the subnanometer and submicrometer ranges. In addition, the structure of such systems at low temperatures has not been investigated in detail, whereas such information is essential for the mechanistic understanding of cryopreservation and related phenomena.

In this study, we investigate concentrated sorbitol–water solutions using variable temperature neutron and X-ray scattering measurements. The combination of small- and wide-angle neutron scattering measurements has been demonstrated to be a powerful tool in studies of the structure of various amorphous systems. The small-angle characterization gives information on the longer-range mesoscopic structure, whereas the wide-angle X-ray and neutron scattering and the associated site-to-site radial distribution function (RDF) analysis give information on the distribution of water molecules on the nanometer scale. Sorbitol is a common pharmaceutical excipient that is used to improve stability of proteins and other drug molecules during freezing, drying, and storage.<sup>11</sup> Even though, like water, sorbitol is a plasticizer because of its relatively low glass transition temperature, a small percentage of sorbitol can significantly increase the stability of dried protein formulations.<sup>12</sup> To investigate the interactions between this

sugar matrix and water, which are amorphous in a typical biopharmaceutical product, a concentration of approximately 70 wt % sorbitol in water is used in these experiments. The concentration is chosen to prevent water crystallization and to ensure that the amorphous structure is maintained at all the temperatures investigated.

To perform a detailed characterization of the structure of concentrated sorbitol–water mixtures on the nanometer length scale, the wide-angle neutron and X-ray scattering (WANS and WAXS) study is carried out in combination with the empirical potential structure refinement (EPSR), which serves to build a structural model of the solution. To investigate the longer-range structure on the length scale of tens and hundreds of nanometers (mesoscopic range structure), small-angle neutron scattering (SANS) experiments are performed. The measurements are carried out in a wide temperature range, both above and below the calorimetric glass temperature,  $T_g$ , which occurs in this system at approximately 200 K.

The WANS studies combined with the EPSR analysis suggest a scenario where the hydroxyl groups in the sorbitol molecules serve to structure the water molecules into well-segregated pockets within the sorbitol matrix. Furthermore, the radial distribution function (RDF) of the water clusters residing in the sorbitol glass was compared with that of the pockets of tetrahedrally bonded low-density amorphous (LDA) ice and the more disordered structure of ambient bulk water. The simulated structure is characterized by pronounced density fluctuations between the sorbitol-rich and water-rich regions even at room temperature. The wide-angle X-ray diffraction patterns also show no sign of crystallization at any temperature, even though the lowest temperature used in this work is 100 K. The hydrogen isotope dependence of the SANS curves implies that the density fluctuations with well-defined interface are occurring on a submicrometer length scale, and these are distinct from the concentration fluctuations at smaller (subnanometer) length scales.

## ■ EXPERIMENTAL SECTION

**Small-Angle Neutron Scattering.** Sorbitol solution samples with different concentrations (w/w) were prepared by adding D-sorbitol(H14) (Sigma, 98% min) and D-sorbitol-(D8) (Cambridge Isotope Laboratories, Cambridge, MA, U.S.A.) to laboratory grade ultrapure Milli-Q water and D<sub>2</sub>O. (Certain equipment or materials are identified in this paper in order to specify the experimental procedure adequately. Such identification is not intended to imply endorsement by the National Institute of Standards and Technology, nor is it intended to imply that the materials or equipment identified are necessarily the best available.) H14 and D8 refer to the natural occurring hydrogen sites and isotopically substituted aliphatic hydrogen sites on sorbitol molecules, respectively. Sorbitol-(H14)–D<sub>2</sub>O (molar fraction of sorbitol 0.187, 67.7 wt %), sorbitol(D8)–D<sub>2</sub>O (68.7 wt %), and sorbitol(H14)–H<sub>2</sub>O (70.0 wt %) were studied. Different isotope contents were chosen to determine whether the substitution of D for H affected the scattering and to reduce the incoherent scattering arising from the presence of H in the sample. To prepare sorbitol–water solutions, the mixtures were heated in closed glass vials until complete dissolution of sorbitol. The SANS measurements were performed on the 30 m SANS instruments<sup>13</sup> at the National Institute of Standards and Technology (NIST), Center for Neutron Research (NCNR) in Gaithersburg, MD. The neutron wavelength,  $\lambda$ , was 6 Å, with a

wavelength spread of  $\Delta\lambda/\lambda \approx 0.15$ . The scattered neutrons were detected with a 64 cm  $\times$  64 cm two-dimensional position-sensitive detector with  $128 \times 128$  pixels at a resolution of 0.5 cm/pixel. The data were reduced using the IGOR program with SANS macro routines developed at the NCNR.<sup>14</sup> The raw counts were normalized to a common neutron intensity and corrected for the empty cell counts, the ambient room background, and the nonuniform detector response. The data obtained from the samples were placed on an absolute scale by normalizing the scattered intensity to the incident beam flux. Finally, the data were radially averaged to produce the scattered intensity,  $I(q)$ , versus  $q$  curves, where  $q = 4\pi \sin(\theta)/\lambda$  and  $2\theta$  corresponds to the scattering angle. Sample-to-detector distances of 12.5, 4.0, and 1.3 m were used for the measurements to cover the  $q$  range between 0.007 and 0.3  $\text{\AA}^{-1}$ . The samples were loaded into demountable 1 mm path length titanium cells with Ti windows. The samples were cooled from 298 to 213, 170, and 100 K and then heated up to 170, 213, and 298 K. The samples were allowed to remain at each temperature for 30 min before each measurement. Data were recorded for the samples at 1.3, 4, and 12.5 m for 5, 10, and 15 min, respectively.

The data obtained are consistent with Porod scattering, and a background (incoherent scattering cross section which is a constant or  $q$ -independent) is added to the coherent scattering level.

The data obtained are consistent with power law scattering

$$I(q) = A q^{-p} + B \quad (1)$$

where  $A$ ,  $B$ , and  $p$  are fitting parameters. The background term,  $B$ , mostly arises from the incoherent scattering from hydrogen in the sample. The data were fit to this equation using the NCNR IGOR SANS data analysis package,<sup>14</sup> and curve fitting was accomplished using the power law model fitting function, defined in eq 1. On the basis of the power law exponent value,  $p$ , morphologies of the scattering domains can be identified as follows:  $p = 4$  corresponds to a sharp interface,  $3 < p < 4$  corresponds to a surface fractal, and  $2 < p < 3$  corresponds to a mass fractal.<sup>15</sup>

**Wide-Angle Neutron Scattering.** The variable temperature wide-angle neutron scattering (WANS) experiments were carried out on the SANDALS diffractometer<sup>16</sup> at the ISIS Facility in the U.K.<sup>17</sup> The experiments were performed on samples with different combinations of isotopic H/D substitution to extract information on the selected site–site radial distribution functions,  $g(r)$ . Three mixtures were studied: sorbitol(H14)–H<sub>2</sub>O mixture, sorbitol(H14)–D<sub>2</sub>O mixture, and sorbitol(D8)–D<sub>2</sub>O. The mole fraction of sorbitol in each of the samples was kept at around 0.19. Each sample was injected into a 1 mm Ti–Zr sample container immersed in a liquid He cooled cryostat and subsequently subjected to a temperature cycle that started out at 298 K and slowly ramped down to 213, 173, 100, and then back to 298 K. The temperature was ramped at a rate of approximately 1 K/min and equilibrated for 1–2 h before the neutron scattering data were collected. In addition, background scattering of the empty containers and a vanadium sample were used as references for putting the data on an absolute scale of scattering cross section.

The Gudrun suite of programs developed by the ISIS disordered materials group<sup>18</sup> has been used for data analysis. The program corrects for multiple scattering, absorption, and inelasticity effects, along with subtraction of the scattering from the sample container and data reduction to an absolute scale. A

detailed description of the procedure can be found elsewhere.<sup>18,19</sup> The EPSR<sup>20</sup> scheme was used to systematically refine the structural model to give the best overall agreement with the diffraction data. The EPSR method builds a simulation box with the same density and composition as the real sample using a reference interaction potential, which incorporates the distinctive characteristics of the system in question. Once the simulation has reached equilibrium using the reference potential on its own, a perturbation to the reference potential, called the empirical potential, derived directly from the diffraction data, is introduced and used to drive the simulated diffraction patterns as close as possible to the measured data.

For the EPSR simulation, the reference potential for the water molecule is derived from that used recently for simulations of pure water,<sup>20</sup> with atom labels Ow and Hw. The sorbitol molecule was divided into four types of atoms, namely, 1C, 1O, 1H, and 2H. The 1H atoms formed the OH bonds, whereas the 2H atoms formed the CH bonds. The 1C atoms were given a Lennard-Jones potential of  $\epsilon = 0.8$  kJ/mol,  $\sigma = 3.7$   $\text{\AA}$ , whereas the 1O and Ow atoms had  $\epsilon = 0.3$  kJ/mol,  $\sigma = 3.2$   $\text{\AA}$ . The Lennard-Jones parameters for 1H, 2H, and Hw were set to zero for these atoms. Charges of  $-1e$ ,  $+0.5e$ ,  $-0.5e$ , and  $+0.5e$  were placed on the Ow, Hw, 1O, and 1H atoms, respectively, to generate hydrogen bonding between neighboring oxygen atoms. These values applied to pure water give very similar structure of water compared to the diffraction data, with a reasonable energy and pressure.<sup>20</sup> The simulated structure of the sorbitol molecule was guided by the single-crystal structure of sorbitol dimers,<sup>21</sup> but internal dihedral flexibility was allowed so that the idealized structure as observed in the single-crystal structure would occur only on average in the simulation—the individual sorbitol molecules might look somewhat different at any instant in time. Each simulation box contained a total of 1000 molecules, in the mole ratio 190 sorbitol to 810 water molecules. Simulations were performed at 298, 213, 173, and 100 K, at assumed number densities of 0.1165 atoms/ $\text{\AA}^3$  at 298 and 213 K, 0.1205 atoms/ $\text{\AA}^3$  at 173 K, and 0.1213 atoms/ $\text{\AA}^3$  at 100 K (details are provided as Supporting Information). The simulations were typically run for approximately 5000 Monte Carlo iterations, where one Monte Carlo iteration consists of five attempted moves of every atom or molecule in the simulation box, and the step is set so that approximately 25% of the attempted moves are accepted. Hence, after each Monte Carlo iteration there was a reasonable assurance that every atom or molecule will have changed position and orientation at least once. After some initial fluctuations, the energy, pressure, and  $\chi^2$  (fit factor) stabilized after 1000–1500 Monte Carlo iterations and remained stable thereafter, with no sign of drift or large excursions. In addition, in EPSR the potential is continually being adjusted by small amounts, and the resulting ensemble-averaged  $g(r)$ s are generally smooth, which means that they have sampled a wide range of molecular configurations which are compatible with the experimental data. Therefore, we have a reasonable confidence that the simulations reached a stationary point. In addition to the neutron scattering data sets, wide-angle X-ray data obtained at the European Synchrotron Radiation Facility (ESRF) on beamline ID-31 on the 70 wt % sorbitol(H14)–H<sub>2</sub>O solution were used for the EPSR simulations at 298 K.

**Wide-Angle X-ray Diffraction.** The high-resolution wide-angle X-ray experiment was carried out for 70% sorbitol/30% water (w/w) at the ESRF on the ID-31 beamline at the X-ray wavelength of 0.79986  $\text{\AA}$ . The sample was prepared in a 1.5

mm borosilicate glass capillary, and the X-ray diffraction pattern was collected at 100 K. This data set was used to confirm the absence of macroscopic crystallization and in the analysis of the WANS data for the structure refinement.

**Differential Scanning Calorimetry.** Differential scanning calorimetry (DSC) analysis was performed with a TA Instruments modulated DSC Q1000 equipped with a refrigerated cooling system. Nitrogen was used as the purge gas with a flow rate of 50 mL/min. Calibration was performed using indium metal as the standard. Samples were sealed in aluminum hermetic pans, cooled to 183 K, and heated at rate of 1 K/min. The scan was modulated with amplitude of 0.5 K and a period of 100 s. Four solutions, i.e., sorbitol(D8)–D<sub>2</sub>O, sorbitol(H14)–D<sub>2</sub>O, sorbitol(H14)–H<sub>2</sub>O, and sorbitol(D8)–H<sub>2</sub>O, were measured. The mole fraction of sorbitol was 0.187 in all four samples, whereas the weight fractions were 0.687, 0.677, 0.7, 0.709, respectively. The T<sub>g</sub> events were detected in all four samples at 200.9, 203.2, 203.0, and 202.0 K (midpoints), respectively, whereas no thermal events that may be associated with sorbitol and/or water crystallization were observed.

## RESULTS

**Small-Angle Neutron Scattering.** The SANS profiles for 70 wt % solutions of (a) sorbitol(H14)–D<sub>2</sub>O, (b) sorbitol(D8)–D<sub>2</sub>O, and (c) sorbitol(D8)–H<sub>2</sub>O in the temperature range of 298–100 K are shown in Figure 1. Table 1 lists the average scattering lengths per atom for sorbitol, water, and the whole sample, for each of these samples, as well as the square of the average scattering length and the observed scattering level at the low-*q* limit (i.e., at  $q = 0.00347 \text{ \AA}^{-1}$ ) for each of the data sets. As one would expect, the high-*q* background in sample b, sorbitol(D8)–D<sub>2</sub>O, is lower due to the smaller number of hydrogen atoms in the system.

In the sorbitol(H14)–D<sub>2</sub>O and sorbitol(D8)–D<sub>2</sub>O samples, identical temperature trends are observed, i.e., the scattering does not change after cooling to 213 K, whereas further cooling to 170 K and then to 100 K results in a significant increase in the scattering intensity. The third sample, sorbitol(D8)–H<sub>2</sub>O, has a similar behavior with one exception, namely, the scattering does not change between 213 and 170 K and increased only after cooling to 100 K. When the samples were heated from 100 K back to 298 K, the scattering intensity decreases but the changes in the scattering intensity with temperature are not entirely reversed. A higher scattering intensity was observed at 298 K for samples at the end of the cooling–heating cycle, as compared with the initial scattering intensity at 298 K in the beginning of the temperature cycle. The scattering intensity curves  $I(q)$  were fit to eq 1 to determine the power law exponent, *p*. The *p* values at 173 and 100 K (i.e., at temperatures when a significant increase in the scattering was observed) fell into the range of 3.8–4.0, implying scattering from well-defined interfaces.

These findings, which show a significant and consistent change in long-range scattering at low temperatures well below the T<sub>g</sub>, were somewhat unusual and unexpected. An obvious reason for the increase in small-angle scattering signal would be from crystallization events which may occur in a sample with decreasing temperature. However, the wide-angle neutron and X-ray experiments demonstrate that the sample remains completely amorphous when cooling to 100 K. In addition, the DSC data have only a glass transition event and do not show any evidence of crystallization or melting (DSC curves

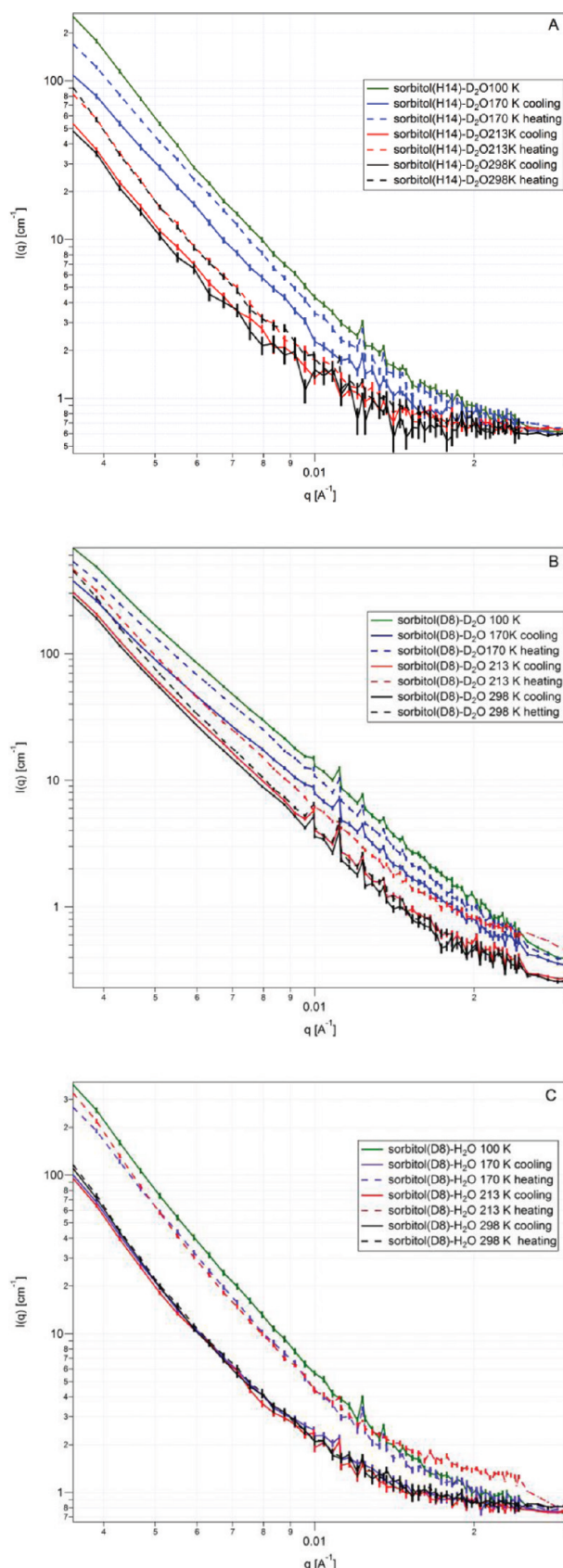


**Figure 1.** SANS patterns of (A) sorbitol(H14)–D<sub>2</sub>O, (B) sorbitol(D8)–D<sub>2</sub>O, and (C) sorbitol(D8)–H<sub>2</sub>O mixtures at different temperatures: solid curves, patterns obtained during cooling cycle; dash curves, patterns obtained during subsequent warming cycle. Error

Figure 1. continued

bars on the measured SANS data represent plus and minus the combined standard uncertainty of the data collection.

**Table 1. Mean Scattering Lengths of Sorbitol, Water, and Total for the Different Solutions Used in the SANS Experiments<sup>a</sup>**

| sample                             | sorbitol [fm] | water [fm] | total [fm] | total squared [fm <sup>2</sup> ] | $I(q)$ at the low- $q$ limit at 100 K (cm <sup>-1</sup> ) |
|------------------------------------|---------------|------------|------------|----------------------------------|---|
| (a) sorbitol(H14)–D <sub>2</sub> O | 2.27          | 3.51       | 2.68       | 7.2                              | 280   |
| (b) sorbitol(D8)–D <sub>2</sub> O  | 5.47          | 3.51       | 4.83       | 23.3                             | 650   |
| (c) sorbitol(D8)–H <sub>2</sub> O  | 4.06          | –0.56      | 2.54       | 6.5                              | 330   |

<sup>a</sup>The mean scattering length of the sorbitol is affected by the isotope composition of the water because of the hydroxyl hydrogen exchange with water hydrogen atoms. Also shown are the square of the total scattering length and the observed scattering intensity at the low- $q$  limit from Figure 1.

not shown). Therefore, the increase in the scattering intensity is not caused by any crystallization events occurring in the sample. The physical origin of the small-angle scattering is considered in the Discussion section in some detail.

**Wide-Angle Neutron Scattering.** The measured differential cross sections for the three samples with different isotope composition at 298 K (before and after the cooling cycle) are shown in Figure 2a. Significant differences in the patterns

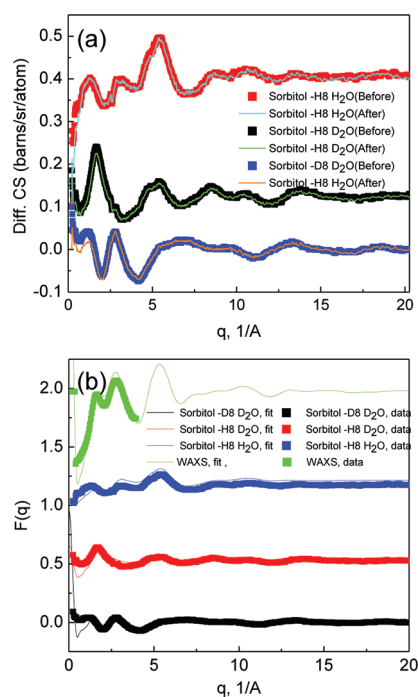


**Figure 2.** WANS pattern of sorbitol–water mixtures. (a) Interference differential cross sections at 298 K before (symbols) and after (lines) cooling. (b) EPSR fits to the combined neutron and X-ray diffraction data at 298 K prior to cooling. The symbols show the data, whereas the line shows the EPSR fits to these data.

between the samples with various D/H ratios were observed, as expected. The differential cross sections obtained at 298 K before (thick lines, Figure 2a) and after cooling (thin lines, Figure 2a) were similar. It should be noted that the high- $q$  limits of the differential cross sections, as reported in Table 2,

**Table 2. Measured Sorbitol–Water Differential Cross Section Levels (barns/sr/atom) in the WANS Experiments**

| temp (K)                          | sorbitol(H14)–D <sub>2</sub> O | sorbitol(H14)–H <sub>2</sub> O | sorbitol(D8)–D <sub>2</sub> O |
|-----------------------------------|--------------------------------|--------------------------------|-------------------------------|
| 298                               | 2.339                          | 3.447                          | 1.323                         |
| 213                               | 2.361                          | 3.476                          | 1.335                         |
| 173                               | 2.281                          | 3.350                          | 1.285                         |
| 100                               | 2.264                          | 3.335                          | 1.280                         |
| 298 (after cooling–heating cycle) | 2.227                          | 3.286                          | 1.268                         |

show a slight drift downward with decreasing temperature to 100 K. Furthermore when warmed back up to 298 K a corresponding restoration of the original level is not observed. Since, in principle, these levels have been normalized to the number of molecules in the neutron beam, a decrease in scattering level would signify a decrease in the amount of material in the neutron beam, although there was no evidence of actual leakage having occurred from the sample containers at the end of the experiment. Although the exact mechanism to explain these observations is unknown, it may be related to the behavior of the small-angle scattering data, where increase in the SANS level was attributed to the formation of microvoids, as described in the Discussion.

Figure 2b shows the EPSR fits at 298 K; similar fits were obtained at other temperatures (curves not shown here). The fitting gives a reasonable description of the experimental data. Note that the simulated curves at all temperatures show a marked rise at low  $q$ . This rise appeared even before the empirical potential (EP) was switched on. Since the lowest available  $q$  in the wide-angle neutron experiment is only 0.2 Å<sup>-1</sup>, and from limitations due to the size of the box used in the EPSR simulation, it is difficult to confirm this rise in the WANS data alone. However, this effect appears to be real, as it does not disappear even after long simulation runs (up to 5000 Monte Carlo iterations), and it is consistent with the SANS results described above.

RDFs for water–water are shown in Figure 3. Although the general appearance of the RDFs does not change much with the temperature, some temperature-related changes are observed. In particular, in both water–water (Figure 3) and sorbitol–sorbitol (not shown) RDFs, the intensity of the first peak increases with cooling, indicative of sharpening sorbitol–sorbitol and water–water correlations, and therefore increased ordering, as the temperature is lowered. However, this effect is much more pronounced in the water–water correlation functions compared to the sorbitol–sorbitol correlations, implying a more rigid sorbitol framework in the simulation. Since no sharp crystalline peaks are observed in either the neutron or X-ray wide-angle patterns, the increase in sorbitol and water ordering is not a result of macroscopic crystallization events. An alternative scenario of a crystalline nanophase, with water forming crystals with very small grain size (of 2 nm size) and therefore with amorphous-like X-ray patterns,<sup>22</sup> is also unlikely, because no melting endotherms were observed in the DSC curves (DSC curves not shown).

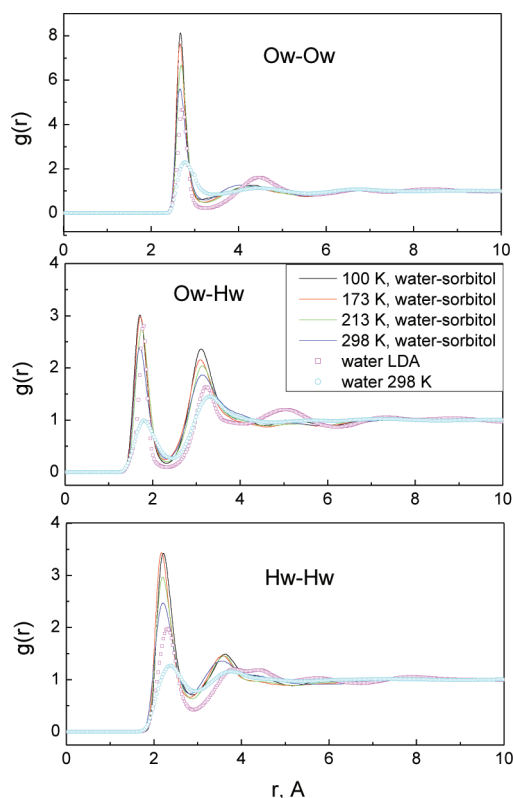


**Figure 3.** Water–water radial distribution functions for sorbitol–water solution (sorbitol mole fraction 0.19, this study) and for pure bulk water and low-density amorphous ice.

## DISCUSSION

**SANS: The Mesoscale Structure.** The SANS patterns shown in Figure 1 correspond to length scales in the range of 20–200 nm. There is little evidence for other than power law scattering at the lowest  $q$ , implying that the characteristic structure has dimensions larger than this limit. In this section, we first consider the temperature trends in SANS, followed by power law analysis to get insight into properties of the scattering structures, and conclude with a discussion on the physical nature of the scattering. In the SANS experiments, the higher- $q$  scattering level is similar at 298 and 213 K and increases after cooling to 170 K.

The temperature dependence of the SANS shows an interesting, and unexpected, trend, i.e., a significant increase in the scattering intensity during a cooling/heating cycle at a temperature below  $T_g$ . Note that the experimental time scale, and therefore the time scale for the SANS changes, was relatively short, of the order of minutes and hours. Moreover, these SANS changes were partially reversed during heating from 100 to 173 K, on the same time scale. Although it is well-known that different types of molecular mobility persist below  $T_g$ , the observation of major scattering intensity changes on the time scale of approximately  $10^2$  min at  $T_g - T = 90$  K, with corresponding inhomogeneities with length scales on the order of tens and hundreds of nanometers, is unusual. Indeed, the structural relaxation time for a typical organic glass at  $T_g - T = 50$  K is on the order of  $10^6$  min or more<sup>23</sup>—which is several orders of magnitude longer than the time scale of changes observed in the present study.

To identify the nature of these low-temperature changes, it is worth comparing the small-angle scattering trends for the

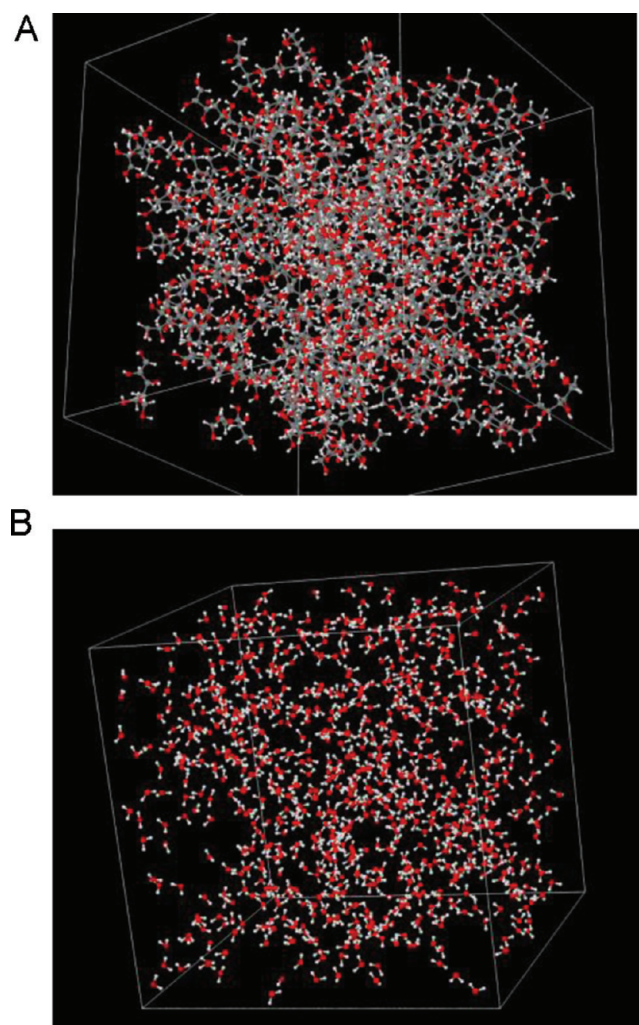


**Figure 4.** (A) Simulation box showing sorbitol molecules in the sorbitol–water system (sorbitol mole fraction 0.19). (B) Simulation box showing water molecules in the sorbitol–water system (sorbitol mole fraction 0.19).

different samples with their corresponding average scattering length. In particular, if the rise in scattering at low  $q$  were caused by increased segregation between water and sorbitol, then it might be expected that sample c (Table 2), which has the largest scattering length contrast between sorbitol and water, would show the largest rise at low  $q$ . In fact it is sample b which shows the largest rise: this sample also has the largest overall scattering length, Table 1. In addition it should be noted that sample a, which has almost the same overall scattering length as sample c but much less contrast between water and sorbitol, has a similar, albeit slightly lower, low- $q$  limit to the scattering. We propose therefore, given the near Porod nature of the low- $q$  scattering, that the SANS changes are related primarily to longer-range voiding on the scale of hundreds of nanometers which in turn give rise to density fluctuations on this length scale, which become more marked as the temperature is lowered. Most likely, the voids represent areas with lower proton density than the condensed sorbitol/water matrix, filled with water vapor and air. Due to the high viscosity of the material, these structures take a long time to equilibrate back to the previously observed higher temperature state once the temperature is raised. Such voiding might also explain the high- $q$  level changes with temperature observed in the WANS

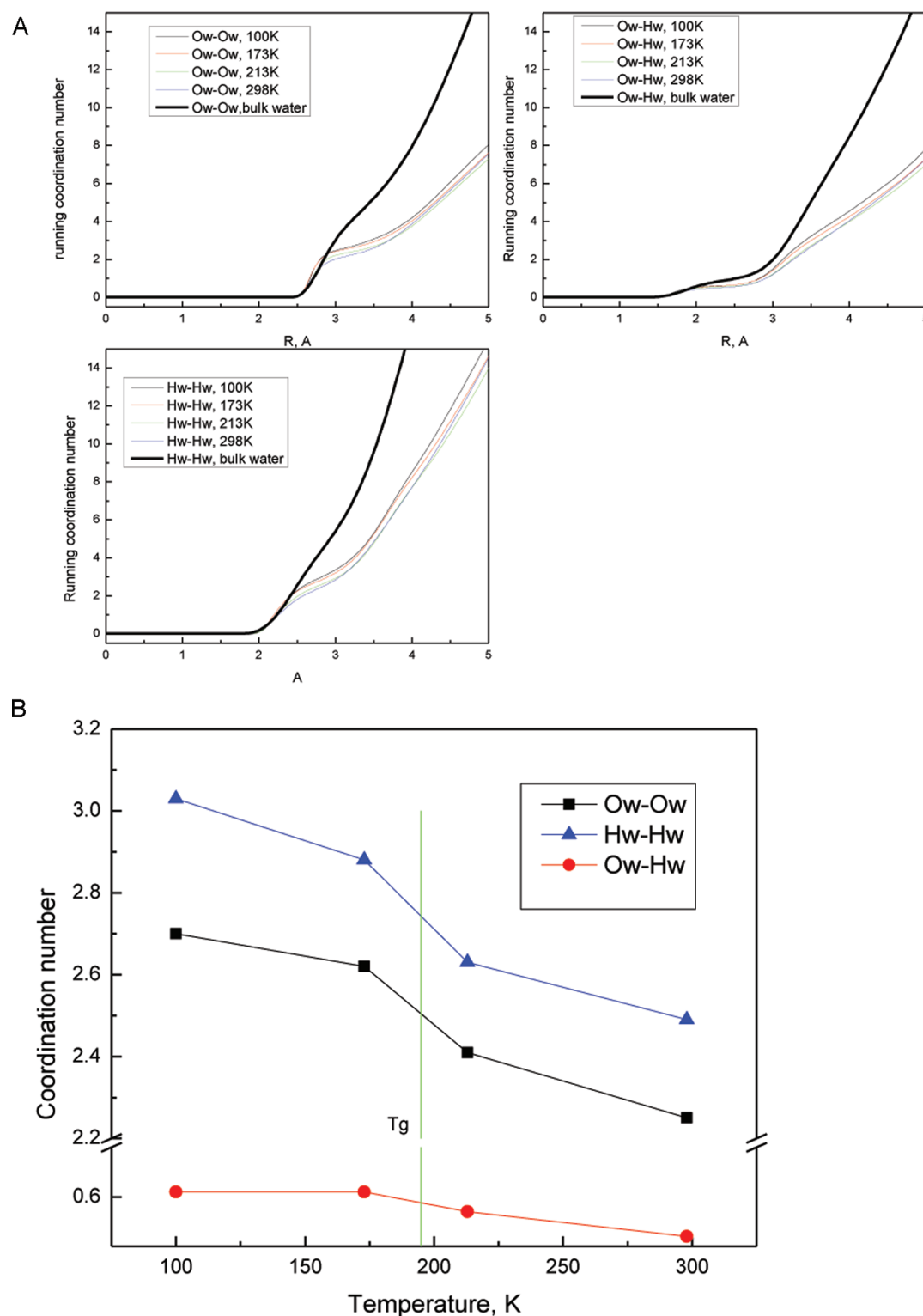


**Figure 5.** (A) Water–water running coordination numbers in the sorbitol–water system (sorbitol mole fraction 0.19). (B) Temperature dependence of the water coordination numbers in the sorbitol–water system (sorbitol mole fraction 0.19).

data, Table 2. At the same time, the slightly increased low- $q$  scattering of sample **c**, with its increased sorbitol/water scattering contrast compared to sample **a**, implies there is also some increased segregation of water and sorbitol at lower temperatures. This is in agreement with WANS observations.

These findings may open new ways into investigations of a wide range of phenomena, such as cold denaturation and

destabilization of proteins, crystallization of organic molecules, and the impact of annealing on the rate of chemical processes, to name a few. For example, interfaces, which were detected by SANS below the  $T_g$ , can be expected to facilitate crystallization of solutes (including cryoprotectors) in aqueous solutions during freezing, which would destabilize proteins. Indeed, crystallization of sorbitol in the frozen solutions, and

**Table 3. Water–Water Coordination Numbers for the Sorbitol–Water System (70 wt % Sorbitol) and Pure Water<sup>a</sup>**

| system, temp (K)        | coordination numbers |       |       |
|-------------------------|----------------------|-------|-------|
|                         | Ow–Ow                | Ow–Hw | Hw–Hw |
| sorbitol–water, 298     | 2.00                 | 0.93  | 2.23  |
| sorbitol–water, 213     | 2.12                 | 1.01  | 2.34  |
| sorbitol–water, 173     | 2.11                 | 1.01  | 2.34  |
| sorbitol–water, 100     | 2.23                 | 1.08  | 2.47  |
| water, 298 <sup>b</sup> | 4.03                 | 1.71  | 4.45  |

<sup>a</sup>Coordination numbers were obtained at radius values corresponding to the first minimum on the RDFs after the peak for sorbitol–water data at 298 K, namely, 3.21, 2.34, and 2.83 Å for Ow–Ow, Ow–Hw, and Hw–Hw, respectively. The coordination numbers for pure water are shown for comparison [from data reported previously (ref 20)].

<sup>b</sup>Ref 20.

corresponding degradation of proteins, has been observed recently.<sup>11a</sup> Potential mechanisms on how interfaces facilitate crystallization processes in glasses below the T<sub>g</sub> have also been described recently by Zhu et al., who reported that the molecular mobility at the interface is many orders of magnitude higher than in the bulk.<sup>24</sup> Furthermore, in protein-containing glasses (e.g., freeze-dried proteins), the appearance of new interfaces is expected to impose additional stresses on proteins, as destabilization of proteins is often associated with interfaces.<sup>25</sup> Finally, in liposomes and biological membranes, it has been suggested, albeit without a direct experimental evidence, that cooling below the T<sub>g</sub> may result in destabilization as a result of mechanical stresses due to fractures and interfaces.<sup>26</sup>

#### WANS: Structure on the Nanometer Length Scale.

Analysis of the WANS data allows us to investigate local structure in water–sorbitol mixtures (including distribution of water molecules) on the nanometer length scale. Figure 4 represents examples of the simulation box showing sorbitol (Figure 4A) and water (Figure 4B) molecules, with nanoscaled voids showing up in the sorbitol matrix (Figure 4A) and a corresponding clustering of water molecules (Figure 4B). To provide a more quantitative view of the water distribution in this system, coordination numbers for both sorbitol–water and pure bulk water are presented in Figure 5A and Table 3. The number of water neighbors around any given water molecule in the water–sorbitol samples is typically about half that of the pure bulk water, suggesting that many water molecules are bonded to sorbitol molecules instead of other water molecules. However, the coordination numbers are also indicative of extensive water–water contacts, i.e., water clusters, with clusters defined as water molecules with Ow–Ow coordination number >1. Coordination numbers increased with cooling, showing further enhancement of water–water contacts at lower temperatures. The same trend can be seen in the water–water RDFs (Figure 3), in which the sharpening of the first peak is also consistent with increased ordering at lower temperatures. Finally, temperature dependence of the coordination numbers (Figure 5B) shows that there is a change in the slope between 213 and 173 K. Although the limited number of temperature data points does not allow the temperature corresponding to this change to be precisely determined, we note that the change in the coordination number temperature dependence is observed in the same temperature region as the calorimetric T<sub>g</sub> and the onset of changes in SANS during cooling.

Furthermore, it is interesting to compare the structure of the clusters of water molecules in sorbitol–water system with structure of two common amorphous forms of water, i.e., liquid water at ambient temperature and LDA. Overlays of the RDFs of water–water in the sorbitol–water mixture with RDFs of bulk liquid water at 298 K and LDA at 80 K are shown in Figure 3. The water–water RDFs in the 70 wt % sorbitol mixture are closer to those in the LDA than to bulk water, based on the strength and position of the first peak. However, there is a difference in the position of the second peak (considered to be a signature of the tetrahedral structure), which is shifted to lower *r* values in the water–sorbitol system, corresponding to a tighter packing of water molecules in the sorbitol matrix as compared to the LDA structure.

The results for the sorbitol–water system are qualitatively similar to those of previous studies of concentrated methanol–water and ethanol–water systems, which showed water clustering and molecular-scale partial demixing between water and cosolvent molecules, due to negative entropy of mixing.<sup>27a</sup> In addition, water clusters in both alcohol–water and sorbitol–water systems appear to be compressed, based on the shift of second RDF peak observed in both cases, although the shift seems to be more dramatic in the alcohol–water systems. On the other hand, similar water clusters were not observed in another relevant system, glycerol–water, possibly because of the lower water concentration (approximately 5 wt %) in the glycerol system studied.<sup>27b</sup> It would be reasonable to suggest that there should be a threshold in the water content associated with a transition from the “water clusters” structure to a more homogeneous distribution of water molecules. Indeed, indirect evidence for such a “clusters/isolated molecules” transition has been obtained in a thermally stimulated current study of sorbitol glasses at variable water levels, with the water content threshold estimated to be at approximately 10 wt %.<sup>28</sup>

## CONCLUSION

In this study, we use small-angle neutron scattering and wide-angle X-ray and neutron scattering to investigate the structure of concentrated sorbitol–water mixtures at different temperatures, both above and below the glass transition temperature. It is found that water molecules form clusters on the nanometer length scale, whereas longer-scale heterogeneity (length scale >200 nm) develops during cooling to below the calorimetric T<sub>g</sub>. These large-scale inhomogeneities, while they occur on the experimental time scale of minutes and hours, are not completely reversible during cooling–heating cycles. Hence water–sorbitol mixtures below the T<sub>g</sub> can be visualized as mesoscaled sorbitol–water domains separated by well-defined interfaces. Within each domain there is increased segregation of water and sorbitol, although at no point do the water clusters become large enough for crystallization to occur. On the subnanometer length scale, water molecules form clusters surrounded by sorbitol molecules which are more structured compared to the bulk form of water and resemble the LDA structure, with water molecules interacting with both water neighbors and sorbitol molecules. Finally, relatively fast structural changes were detected by both WANS and SANS well below the calorimetric T<sub>g</sub>. Although there are reports on molecular mobility below the T<sub>g</sub> by such methods as enthalpy relaxation,<sup>29</sup> NMR,<sup>30</sup> and elastic neutron scattering,<sup>31</sup> this study is a rare report on structural changes which take place at temperatures well below the T<sub>g</sub> on both nanometer and

submicrometer length scales with a relative short time scale of minutes and hours.

## ■ ASSOCIATED CONTENT

### ■ Supporting Information

Estimation of the density of the sorbitol–water mixture. This material is available free of charge via the Internet at <http://pubs.acs.org>.

## ■ AUTHOR INFORMATION

### Corresponding Author

\*E-mail: [shalaev\\_evgeniyi@allergan.com](mailto:shalaev_evgeniyi@allergan.com).

### Present Address

<sup>1</sup>Allergan Inc., 2525 Dupont Dr., Irvine, CA 92612.

### Notes

The authors declare no competing financial interest.

## ■ ACKNOWLEDGMENTS

Experiments at the ISIS Pulsed Neutron and Muon Source were supported by a beam time allocation from the Science and Technology Facilities Council. This work utilized facilities (NCNR) supported in part by the National Science Foundation under agreement no. DMR-0944772. S.G.C. and S.K. gratefully acknowledge partial support from the National Research Council. E.Y.S. gratefully acknowledges Dr. Simon Bates for preliminary analysis of the data using radial distribution function (not included in the manuscript) and Dr. Yuriy Abramov for helpful discussion on RDFs. S.K. gratefully acknowledges Dr. Paul Butler for help in SANS experiments and Dr. Boualem Hammouda for helpful discussions on interpretation of SANS results. The authors thank Drs. Theyencheri Narayanan and Michael Sztucki of ESRF for very useful discussions of small-angle scattering.

## ■ REFERENCES

- (1) (a) Crowe, J. H.; Crowe, L. M.; Jackson, S. A. *Arch. Biochem. Biophys.* **1983**, *220* (2), 477–484. (b) Crowe, L. M. *Comp. Biochem. Physiol., Part A: Mol. Integr. Physiol.* **2002**, *131* (3), 505–513. (c) Koster, K. L. *Plant Physiol.* **1991**, *96* (1), 302–304.
- (2) (a) Carpenter, J. F.; Pikal, M. J.; Chang, B. S.; Randolph, T. W. *Pharm. Res.* **1997**, *14* (8), 969–975. (b) Tang, X. L.; Pikal, M. J. *Pharm. Res.* **2004**, *21* (2), 191–200. (c) Levine, H.; Slade, L. In *Water Science Reviews*; Franks, F., Ed.; Cambridge University Press: Cambridge, U.K, 1988; Vol. 3, pp 79, 185.
- (3) Franks, F. *Pure Appl. Chem.* **1997**, *69* (5), 915–920.
- (4) Franks, F. *Cryo-Lett.* **1990**, *11* (2), 93–110.
- (5) (a) Strambini, G. B.; Gonnelli, M. *Biophys. J.* **2007**, *92*, 2131–2138. (b) Varshney, D. B.; Elliott, J. A.; Gatlin, L. A.; Kumar, S.; Suryanarayanan, R.; Shalaev, E. Y. *J. Phys. Chem. B* **2009**, *113* (18), 6177–6182.
- (6) Dong, J. P.; Hubel, A.; Bischof, J. C.; Aksan, A. *J. Phys. Chem. B* **2009**, *113* (30), 10081–10087.
- (7) (a) Girlich, D.; Ludemann, H. D. *Z. Naturforsch., C: Biosci.* **1994**, *49* (3–4), 250–257. (b) Roberts, C. J.; Debenedetti, P. G. *J. Phys. Chem. B* **1999**, *103* (34), 7308–7318.
- (8) (a) Cordone, L.; Cottone, G.; Giuffrida, S. *J. Phys.: Condens. Matter* **2007**, *19* (20), 16. (b) Molinero, V.; Cagin, T.; Goddard, W. A. *J. Phys. Chem. A* **2004**, *108* (17), 3699–3712.
- (9) Molinero, V.; Cagin, T.; Goddard, W. A. *Chem. Phys. Lett.* **2003**, *377* (3–4), 469–474.
- (10) Bordat, P.; Lerbret, A.; Demaret, J. P.; Affouard, F.; Descamps, M. *Europhys. Lett.* **2004**, *65* (1), 41–47.
- (11) (a) Piedmonte, D. M.; Summers, C.; McAuley, A.; Karamujic, L.; Ratnaswamy, G. *Pharm. Res.* **2007**, *24* (1), 136–146. (b) Nash, R. A. In *Handbook of Pharmaceutical Excipients*; Kibbe, A. H., Ed.;

American Pharmacists Association and Pharmaceutical Press: Washington, DC, 2000.

(12) Chang, L.; Shepherd, D.; Sun, J.; Tang, X.; Pikal, M. J. *J. Pharm. Sci.* **2005**, *94* (7), 1445–1455.

(13) Glinka, C. J.; Barker, J. G.; Hammouda, B.; Krueger, S.; Moyer, J. J.; Orts, W. J. *J. Appl. Crystallogr.* **1998**, *31*, 430–445.

(14) Kline, S. R. *Crystallography* **2006**, *39*, 895–900.

(15) Narayanan, T. In *Soft Matter Characterization*; Borsali, R., Pecora, R., Eds.; Springer-Verlag: Berlin, Heidelberg, Germany, 2008; pp 899–952.

(16) Soper, A. K. *Conference on Advanced Neutron Sources*; Hyer, D. K., Ed.; Institute of Physics and Physical Society, Bristol, 1988; pp 353–366.

(17) [www.isis.stfc.ac.uk](http://www.isis.stfc.ac.uk), Science and Technology Facilities Council, accessed April 6, 2012.

(18) <http://www.isis.stfc.ac.uk/groups/disordered-materials/>, accessed April 6, 2012.

(19) Pagnotta, S. E.; McLain, S. E.; Soper, A. K.; Bruni, F.; Ricci, M. A. *J. Phys. Chem. B* **2010**, *114* (14), 4904–4908.

(20) Soper, A. K. *J. Phys.: Condens. Matter* **2007**, *19* (33), 18.

(21) Schouten, A.; Kanters, J. A.; Kroon, J.; Comini, S.; Looten, P.; Mathlouthi, M. *Carbohydr. Res.* **1998**, *312* (3), 131–137.

(22) Mancinelli, R. *J. Phys.: Condens. Matter* **2010**, *22* (40), 404213.

(23) Hancock, B. C.; Shamblin, S. L.; Zografi, G. *Pharm. Res.* **1995**, *12* (6), 799–806.

(24) Zhu, L.; Wong, L.; Yu, L. *Mol. Pharm.* **2008**, *5* (6), 921–926.

(25) Broos, J.; Strambini, G. B.; Gonelli, M.; Wolters, G. S.; Vos, E. P.; Robillard, G. T. *Biophys. J.* **2001**, *80* (1), 258A–258A.

(26) Shalaev, E. Y.; Steponkus, P. L. *J. Phys. Chem. B* **2003**, *107* (34), 8734–8737.

(27) (a) Soper, A. K.; Dougan, L.; Crain, J.; Finney, J. L. *J. Phys. Chem. B* **2006**, *110* (8), 3472–3476. (b) Towey, J. J.; Soper, A. K.; Dougan, L. *Phys. Chem. Chem. Phys.* **2011**, *13* (20), 9397–9406.

(28) Ewing, S.; Hussain, A.; Collins, G.; Roberts, C. J.; Shalaev, E. Y. In *Water Stress in Biological, Chemical, Pharmaceutical and Food Systems*; Gutiérrez, G., Alamilla, L., Eds; in press.

(29) Liu, J. S.; Rigsbee, D. R.; Stotz, C.; Pikal, M. J. *J. Pharm. Sci.* **2002**, *91* (8), 1853–1862.

(30) Yoshioka, S.; Aso, Y.; Kojima, S. *Pharm. Res.* **1996**, *13* (6), 926–930.

(31) Cicerone, M. T.; Soles, C. L. *Biophys. J.* **2004**, *86* (6), 3836–3845.